Inorganic Chemistry

pubs.acs.org/IC

Article

N-Heterocyclic Carbene Gold Complexes in a Photocatalytic CO_2 Reduction Reaction

Dinesh Nugegoda, Nikolaos V. Tzouras, Steven P. Nolan,* and Jared H. Delcamp*

Cite This: *Inorg. Chem.* 2022, 61, 18802−18809

Read Online

ACCESS | Metrics & More | Article Recommendations | Supporting Information

ABSTRACT: Molecular catalysts that are durable and highly selective in the photocatalytic CO_2 reduction reaction (PCO_2RR) are in high demand. Molecular gold complexes are underexplored in the CO_2RR manifold despite heterogeneous gold−CO_2 reduction catalyst counterparts being frequently studied. In this report, a series of *N*-heterocyclic carbene (NHC)-ligated Au complexes are evaluated in the PCO_2RR with an added photosensitizer (tris(2-phenylpyridine)iridium, $Ir(ppy)_3$). The complexes were each studied with and without an added activator used to open a coordination site on the Au complexes. Results show an example of an exceptionally durable PCO_2RR catalyst lasting >100 h with high product selectivity for CO. Heterogeneity tests reveal no evidence of a nonhomogeneous active catalyst, and structure−activity relationships of the molecular complexes are discussed.

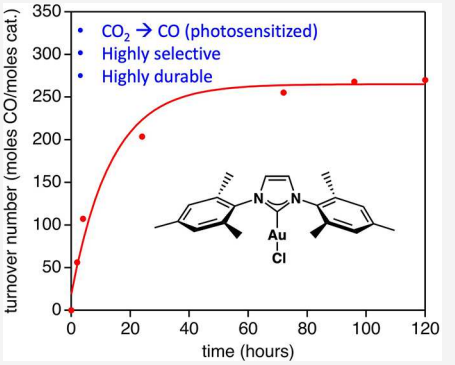

INTRODUCTION

The photocatalytic conversion of CO_2 to reduced carbon states with visible light is a promising direction in renewable energy production.[1−8] The photocatalytic CO_2 reduction reaction (PCO_2RR) is often driven with a photosensitizer (PS) and a transition-metal-based CO_2 reduction reaction (CO_2RR) catalyst.[9,10] Molecular catalysts help to easily make precise structural modifications with atomistic-level control, which enables the rapid iterative design of CO_2RR catalysts through understanding the structure−function relationship. Au-based *N*-heterocyclic carbene (NHC)-ligated molecular catalysts are underexplored in the PCO_2RR despite these complexes being of interest for a large variety of transformations such as C−H activation, alkyne hydration, nitrile hydration, and alkene activation among others.[11−27] In general, NHC ligands are strong sigma donors with variable stereochemical and electronic features, capable of covalently bonding to a gold center to give, in many cases, more reactive catalysts with enhanced durability which are needed characteristics in the PCO_2RR.[13,28]

In general, molecular Au catalysts in the PCO_2RR are underexplored, and our group reported the first examples.[29] This is in sharp contrast to the large number of studies on Au heterogeneous catalysts and Au nanoparticles in the CO_2 reduction literature.[30−37] Among the five molecular catalysts originally reported, one NHC-ligated Au complex was evaluated, showing relatively moderate performance in the PCO_2RR with promising electrochemical reactivity observed under a CO_2 atmosphere. In this work, we seek to understand the effects of NHC ligand tuning both sterically and electronically on the PCO_2RR with Au complexes (Figure 1). Additionally, varying the ligand which dissociates to open a reactive site has not been studied with Au−NHC complexes, and we seek to understand the effects of this ligand on catalyst activity in the PCO_2RR. This report studies the performance of eleven Au−NHC complexes that differ in the wingtip substituents on the NHC ligand, the saturated or unsaturated backbone in the NHC ligand, and the labile ligand (counterion) on the Au center (Figure 1).

Six of the complexes evaluated in the PCO_2RR have an imidazole NHC ligand with 2,6-diisopropylphenyl (IPr) wingtips. These complexes are all numbered as **1**, with superscripts denoting the labile ligands on each Au complex. Specifically, chloride ($\mathbf{1}^{Cl}$), hydroxide ($\mathbf{1}^{OH}$), bis(trifluoromethane)sulfonamide ($\mathbf{1}^{NTf2}$), tetrafluoroborate ($\mathbf{1}^{BF4}$), carbazole ($\mathbf{1}^{Cz}$), and a hydroxide-bridged bimetallic complex ($\mathbf{1}^{OH}\mathbf{1}^{BF4}$) were selected to evaluate the effects of a range of labile ligand binding strengths and counterions on the PCO_2RR reaction. Interestingly, $\mathbf{1}^{OH}$ and $\mathbf{1}^{OH}\mathbf{1}^{BF4}$ combined are known to trap CO_2 stoichiometrically.[38] Complexes $\mathbf{2}^{Cl}$, $\mathbf{3}^{Cl}$, and $\mathbf{4}^{Cl}$ vary the wingtip groups as mesityl (Mes), 2,6-dibenzhydryl-4-methyl phenyl (IPr*), and adamantyl (Ad), respectively. These wingtip changes seek to probe the effects of varied steric and electronic characteristics on the Au catalysts during the PCO_2RR.[39] $\mathbf{4}^{Ph}$ is also evaluated in the PCO_2RR to

Received: October 2, 2022
Published: November 9, 2022

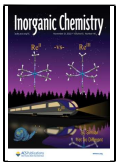

https://doi.org/10.1021/acs.inorgchem.2c03487
Inorg. Chem. 2022, 61, 18802−18809

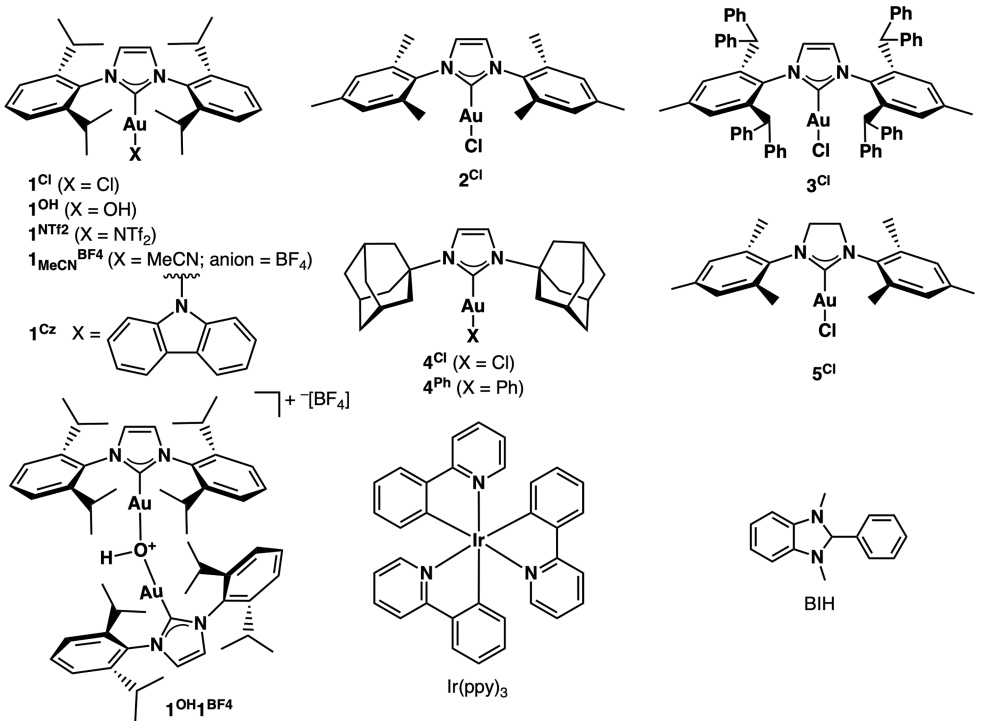

Figure 1. Structures of Au−NHC complexes, photosensitizer, and sacrificial electron donor.

compare with $\mathbf{4}^{Cl}$ to analyze the difference in the dissociation of a chloride versus benzene (once protonated). Finally, $\mathbf{5}^{Cl}$ is comparable to $\mathbf{2}^{Cl}$ since both complexes have chloride ligands and Mes wingtips on the NHC ligand but vary at the imidazolylidene ring with $\mathbf{5}^{Cl}$ being saturated along the ligand backbone.

In all experiments, the photosensitizer (PS) is $Ir(ppy)_3$ (where ppy is 2-phenylpyridine) since this complex is a potent reductant upon addition of an electron to give $[Ir(ppy)_3]^-$ (Figure 2).[40] $Ir(ppy)_3$ has a higher driving force for electron transfer than many PSs used in the PCO_2RR, which allows for the probing of a wide range of catalysts under similar conditions. 1,3-Dimethyl-2-phenyl-2,3-dihydro-1*H*-benzo[*d*]-imidazole (BIH) is used as a sacrificial electron donor (SED) in all of the PCO_2RRs due to the strongly reducing nature of BIH relative to other commonly used SEDs such as alkylamines.[40] Notably, triethylamine is added to these reactions to deprotonate $BIH^{\bullet+}$ after electron transfer to photoexcited $Ir(ppy)_3$ to promote an irreversible electron transfer event (Figure 2).[5,41] All reactions evaluated here are photosensitized as a prior study demonstrated a PS is necessary for the product to be observed with an Au−NHC complex.[29] A proposed catalytic cycle is shown in Figure 2 with the roles of $Ir(ppy)_3$, BIH, TEA, and the Au catalyst depicted. Addition of a Au catalyst to CO_2 upon opening a reactive site is proposed based on prior cyclic voltammetry studies on $\mathbf{1}^{Cl}$ and common observations in the literature that NHC-ligated metals favor the addition of CO_2 after a single electron reduction of the metal complex leading to the opening of a reactive site.[42−46] The series of catalysts being probed in this study also allow analysis of how varied labile ligands promote entry into the catalytic cycle. Additionally, NHC ligand variations allow for probing of how the addition of Au complexes to CO_2 and the subsequent protonation, C−O bond cleavage, and CO dissociation steps are affected in the catalytic cycle.

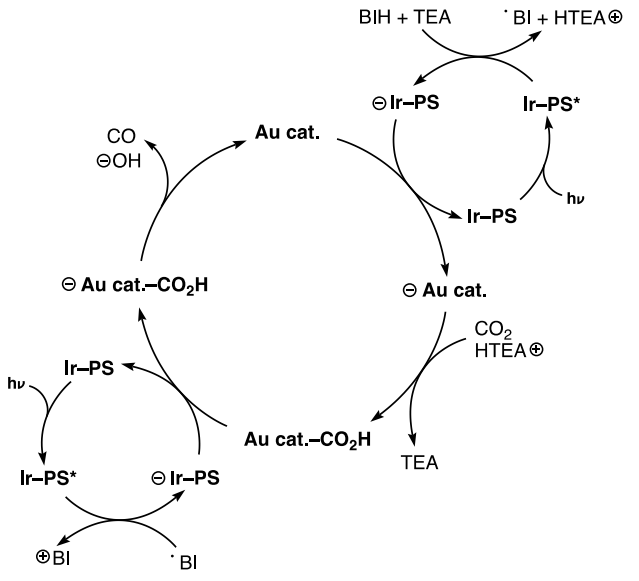

Figure 2. Proposed general catalytic cycle for NHC-ligated Au complexes in the PCO_2RR. BIH conversion to $^{\bullet}BI$ and ^{+}BI has been previously discussed in the literature.[5,41]

RESULTS AND DISCUSSION

Catalyst Synthesis. All complexes were synthesized via literature methods and their purity confirmed through elemental analysis.[47−53] See the Experimental Section below for specific complex references.

Photocatalytic CO_2 Reduction. Unless otherwise noted, all PCO_2RRs were conducted with 1 μM Au complex, 100 μM $Ir(ppy)_3$, 0.02 M BIH, and 5% v/v TEA in dry acetonitrile. The reaction mixtures were irradiated with a white LED (380−750 nm range) set to a power density of 63.6 mW/cm^2. All of the

https://doi.org/10.1021/acs.inorgchem.2c03487
Inorg. Chem. 2022, 61, 18802−18809

Table 1. Data with Varied Au Complexes and Activators in the PCO_2RR[a]

Au cat.	activator	TON (CO)	TOF_1 (h^{-1})	TOF_M (h^{-1})	TOF_F (h^{-1})
$\mathbf{1}^{Cl}$		23 ± 7	5.6 ± 0.0	5.6 ± 0.0	0.1 ± 0.0
$\mathbf{1}^{Cl}$	$AgBF_4$	22 ± 6	4.6 ± 2.6	4.6 ± 2.6	0.3 ± 0.2
$\mathbf{2}^{Cl}$		45 ± 9	8.4 ± 1.0	8.4 ± 1.0	0.0 ± 0.0
$\mathbf{2}^{Cl}$	$AgBF_4$	20 ± 4	3.3 ± 0.3	3.3 ± 0.2	0.0 ± 0.0
$\mathbf{3}^{Cl}$		11 ± 9	2.1 ± 0.9	2.1 ± 0.9	0.0 ± 0.0
$\mathbf{3}^{Cl}$	$AgBF_4$	13 ± 2	2.9 ± 0.4	2.9 ± 0.4	0.0 ± 0.0
$\mathbf{4}^{Cl}$		14 ± 3	3.6 ± 0.1	3.6 ± 0.1	0.0 ± 0.0
$\mathbf{4}^{Cl}$	$AgBF_4$	20 ± 8	6.5 ± 1.4	6.5 ± 1.4	0.0 ± 0.0
$\mathbf{5}^{Cl}$		37 ± 4	6.0 ± 1.4	6.0 ± 1.4	0.0 ± 0.0
$\mathbf{5}^{Cl}$	$AgBF_4$	37 ± 12	10.3 ± 1.4	10.3 ± 1.4	0.3 ± 0.4
$\mathbf{1}^{OH}$		23 ± 2	1.0 ± 0.1	1.0 ± 0.1	0.3 ± 0.1
$\mathbf{1}^{OH}$	$HBF_4{*}Et_2O$	20 ± 1	1.5 ± 0.3	1.6 ± 0.0	0.1 ± 0.0
$\mathbf{1}^{NTf2}$		18 ± 4	2.4 ± 1.5	2.4 ± 1.5	0.2 ± 0.1
$\mathbf{1}_{MeCN}^{BF4}$		36 ± 14	4.3 ± 2.8	4.3 ± 2.8	0.5 ± 0.1
$\mathbf{1}^{Cz}$		10 ± 0	0.0 ± 0.0	1.3 ± 0.3	0.1 ± 0.0
$\mathbf{1}^{Cz}$	$HBF_4{*}Et_2O$	25 ± 8	2.5 ± 1.0	2.5 ± 1.0	0.0 ± 0.0
$\mathbf{1}^{OH}\mathbf{1}^{BF4}$		24 ± 6	2.1 ± 0.7	2.1 ± 0.7	0.3 ± 0.2
$\mathbf{4}^{Ph}$		35 ± 16	0.5 ± 0.7	0.8 ± 0.4	0.4 ± 0.2
$\mathbf{4}^{Ph}$	$HBF_4{*}Et_2O$	28 ± 6	3.7 ± 1.1	3.7 ± 1.1	0.0 ± 0.0

[a]Values are reported per Au atom with the complex at 1 μM for $\mathbf{1}^{OH}\mathbf{1}^{BF4}$. TOF_1 is the TOF at 1 h. TOF_M is the maximum TOF observed after 1 h. TOF_F is the TOF at 72 h. See Figures S14 and S15 for TON versus time plots with 90% confidence intervals at all timepoints.

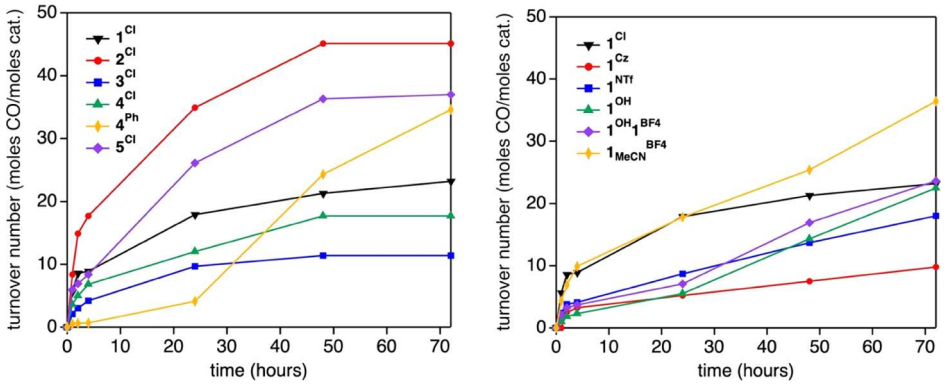

Figure 3. TON of CO versus time plots of the Au complexes in the PCO_2RR. Varied NHC ligands are compared on the left and varied labile ligands are compared on the right. The TON values for $\mathbf{1}^{OH}\mathbf{1}^{BF4}$ are per Au atom with the complex at 1 μM.

reaction mixtures were analyzed for CO, CH_4, H_2, and CO_2H^-, and only CO and trace H_2 (<1 TON) were observed, which indicates high selectivity toward a single carbon-based reduction product. As controls, removal of CO_2, BIH, Au catalyst, or Ir photosensitizer from the reaction led to no CO production. The catalysts were first evaluated without any additives in the reaction mixture for turnover number (TON) values at 72 h (moles of CO/moles of Au complex) and for the turnover frequency per hour (TOF h^{-1}) at 1 h (TOF_1), from the final 48 to 72 h time segment (TOF_F) and at the maximum value observed (TOF_M) (Table 1). TON versus time plots are provided to compare each of the catalysts (Figure 3).

Without an activator, the chloride complexes gave TOF_1 and TON values in the following order: $\mathbf{2}^{Cl} > \mathbf{5}^{Cl} > \mathbf{1}^{Cl} > \mathbf{4}^{Cl} > \mathbf{3}^{Cl}$. The two mesitylene wingtip-bearing complexes had the highest TOF and TON values among the series of chloride complexes with the unsaturated backbone catalyst having appreciably higher TOF_1 and TON (8.4 h^{-1} and 45 vs 6.0 h^{-1} and 37, respectively). The exceptionally bulky wingtip ligand of $\mathbf{3}^{Cl}$ is correlated to the lowest TOF_1 and TON of the series. The two complexes ($\mathbf{3}^{Cl}$ and $\mathbf{4}^{Cl}$) which were slow to dissolve in MeCN were also analyzed in *N,N*-dimethylformamide (DMF) as solvent (Figures S1, S2, and S8). In both cases, DMF gave higher TON values by > 5 turnovers, but the TOF values were significantly higher in the first 2 h with MeCN (Figure S2). Due to the relative ease of using distilled MeCN and the higher initial TOF values, MeCN was used as the comparison solvent for all of the catalysts examined in this study. The catalysts examined here are relatively robust to prolonged photocatalysis compared to systems based on benchmark rhenium NHC and bipyridine complexes that last only 1−2 h under analogous conditions.[43,54] To probe the reason why catalysis halts around 72 h for some catalyst such as $\mathbf{2}^{Cl}$, an experiment with $\mathbf{2}^{Cl}$ was conducted where an additional portion of $Ir(ppy)_3$, BIH, or CO_2 was added at 24 h to probe if any of these reagents were depleted in the reaction (Figure S13). $Ir(ppy)_3$ addition at 24 h was found to significantly increase the rate of catalysis during the 24 to 48 h time frame with a higher overall TON obtained. This indicates the photosensitizer decomposes under these conditions, leading to reduced turnovers.

Comparing varied labile ligands on gold complexes with the common ligand **1** shows the following trend of TOF_1 values

https://doi.org/10.1021/acs.inorgchem.2c03487
Inorg. Chem. 2022, 61, 18802−18809

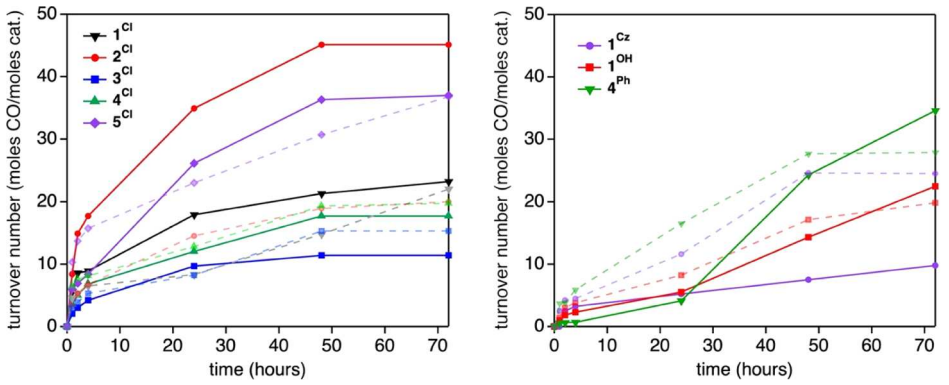

Figure 4. TON of CO versus time plots of the Au complexes in the PCO_2RR with activators added (left: $AgBF_4$; right: HBF_4*Et_2O). Lighter color dashed lines and markers correspond to the PCO_2RR with the activator added and darker colors correspond to no activator added.

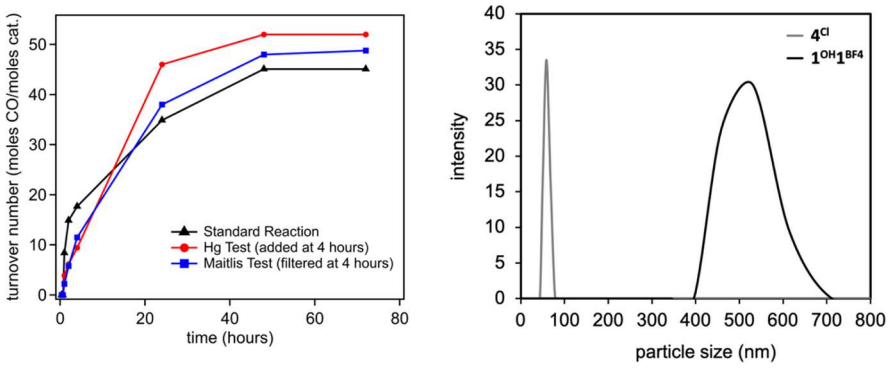

Figure 5. Homogeneity versus heterogeneity probing tests (left: Maitlis and Hg^0 tests with $\mathbf{2}^{Cl}$; right: DLS graph). Maitlis test performed at 4 h is shown by the black trace. Hg^0 added at 4 h is shown by the blue trace. DLS was conducted at 72 h. Catalysts not listed in the DLS legend did not show any signal in the 2−800 nm particle size range.

ranging from 5.6 to 0.0 h^{-1}: $\mathbf{1}^{Cl} > \mathbf{1}_{MeCN}^{BF4} > \mathbf{1}^{NTf2} > \mathbf{1}^{OH} = \mathbf{1}^{OH}\mathbf{1}^{BF4} > \mathbf{1}^{Cz}$ (Figure 3 and Table 1). Chloride-ligated complexes being faster CO_2 reduction catalysts than the presumably MeCN-ligated complexes has been previously attributed to a more easily dissociated anionic ligand upon reduction of the complex.[42] After 72 h, all catalysts retain some activity with TOF_F values ranging from 0.1 to 0.5 h^{-1}. A chloride-labile ligand is compared to a phenyl group via complexes $\mathbf{4}^{Cl}$ and $\mathbf{4}^{Ph}$. This comparison shows a higher TOF_I for the $\mathbf{4}^{Cl}$ catalyst (3.6 h^{-1} vs 0.5 h^{-1}) but a higher TON value for the $\mathbf{4}^{Ph}$ catalyst (35 vs 14 TON). Thus, while the phenyl group does not impart increased rates of reaction, this group does impart increased catalyst durability. Among all catalysts, only $\mathbf{1}^{Cz}$ and $\mathbf{4}^{Ph}$ do not have TOF_I values approximately equal to TOF_M values, which indicates a significant induction period is present until the active catalyst can be formed (Figures S3−S6). Interestingly, $\mathbf{1}^{OH}$ and $\mathbf{1}^{OH}\mathbf{1}^{BF4}$ show general improvements in changes to TOF over time for the time segments after 24 h of irradiation (e.g., the 24−72 h time period relative to the preceding segment from 4 to 24 h).

The presence of an induction period with $\mathbf{1}^{Cz}$ and $\mathbf{4}^{Ph}$ prompted us to explore the role of opening a reactive site on the Au catalysts. Specifically, $AgBF_4$ was used with the chloride complexes to remove the chloride ligand via a metathesis reaction prior to initiating catalysis (Figure 4 and Table 1).[55] HBF_4*Et_2O was used as an acid activator to facilitate the protonation of the labile groups on catalysts $\mathbf{1}^{OH}$, $\mathbf{1}^{Cz}$, and $\mathbf{4}^{Ph}$ to open a coordination site (Figure 4).[53,56] Despite the chloride complex of **1** being a faster CO_2 reduction complex than other chloride-free complex analogues of **1**, chloride complexes $\mathbf{4}^{Cl}$ and $\mathbf{5}^{Cl}$ gave a dramatically positive change in TOF_I rates (∼1.8×) upon $AgBF_4$ activation, which illustrates that the chloride-ligated complexes are not strictly faster catalysts across all ligand frameworks. This indicates that the complexes with alkyl-substituted wingtips or saturated NHC rings are relatively slow to be reduced or dissociate a chloride during the PCO_2RR. However, no dramatic differences are noted in the cyclic voltammetry studies with respect to reduction potential, which suggests the rate of reactivity is not likely due to a sluggish reduction reaction (Figure S7). Thus, the rate of reactivity change may be due to the rate at which a coordination site opens. However, in several cases, the chloride-ligated complexes are faster catalysts such as when a series based on **1** (no activators), **2** with and without an activator, $\mathbf{4}^{Cl}$, and $\mathbf{4}^{Ph}$ are compared. As an example, $\mathbf{2}^{Cl}$ has appreciably higher TOF_I and TON values without the addition of $AgBF_4$ (8.4 h^{-1} and 45 vs 3.3 h^{-1} and 20). Cyclic voltammetry conducted on $\mathbf{2}^{Cl}$ before and after exposure to $AgBF_4$ shows only a moderate shift in the reduction potential onset (∼100 mV), which indicates that the initial electron transfer reaction to reduce the complex is not the likely reason for the nonobvious change in the reactivity observed (Figure S7). A possible explanation for the higher reactivity of $\mathbf{2}^{Cl}$ in the absence of $AgBF_4$ could be due to the transition state which dissociates a Cl^- being lower in energy than a transition state dissociating a MeCN group (present after metathesis) from a single electron reduced complex, as has been observed during electrocatalytic CO_2 reduction studies via density functional theory.[42]

https://doi.org/10.1021/acs.inorgchem.2c03487
Inorg. Chem. 2022, 61, 18802−18809

Acid activation was explored with respect to the PCO_2RR with $\mathbf{1}^{OH}$, $\mathbf{1}^{Cz}$, and $\mathbf{4}^{Ph}$. In all cases, addition of HBF_4*Et_2O led to a faster TOF_1 with the most dramatic effects being observed with $\mathbf{1}^{Cz}$ and $\mathbf{4}^{Ph}$. Additionally, the TOF_1 values and TOF_M values were in close agreement after addition of an acid additive, indicating that the induction period found with $\mathbf{1}^{Cz}$ and $\mathbf{4}^{Ph}$ without HBF_4*Et_2O is no longer present. Higher TON values are observed for all three catalysts through 24 h; however, after 72 h, higher TON values are observed for $\mathbf{4}^{Ph}$ and $\mathbf{1}^{OH}$ without a HBF_4*Et_2O treatment. A plausible explanation for this observation could be due to catalyst−catalyst deactivating interactions which are suspected in the PCO_2RR due to lower concentrations of catalysts commonly being observed to give much higher TON values in many systems.[57−60] Without the presence of an acid activator, the active catalyst could be slow to form and could be slowly released over time, limiting the number of reactive catalyst species present in solution.

The highest TON and TOF_1 catalyst ($\mathbf{2}^{Cl}$) without an activator was studied via a series of experiments to probe for homogeneous versus heterogeneous catalyst behavior since Au nanoparticles/nanomolecules are well documented in CO_2RRs as mentioned in the Introduction. The Maitlis test was conducted by initiating a typical PCO_2RR for 4 h, followed by filtration of the reaction mixture over a bed of Celite under an inert atmosphere via an in-line filtration to remove any suspended nanoparticles.[61,62] The solution was then degassed with CO_2 and photolyzed for 68 more hours (72 h in total; Figure 5). A similar reaction profile is observed with both the unperturbed reaction and the filtered reaction with very similar TON values (56 vs 60 TON at 72 h, respectively). We stress that proving an active catalyst is molecular in nature is not possible;[62] however, this data is consistent with a homogeneous molecular catalyst in the PCO_2RR.

Next, a Hg^0 test was conducted as a second homogeneity test.[62] Importantly, Au−Hg amalgams are well documented, and miscibility of the catalyst metal and Hg is required for the use of this test.[63] A PCO_2RR was initiated with $\mathbf{2}^{Cl}$ for 4 h to generate an active catalyst and then Hg^0 was added to the reaction mixture with the mixture photolyzed for 68 more hours (Figure 5). If the active catalyst was an Au nanoparticle, it is expected that the Au nanoparticle would be dissolved in the Hg^0 layer upon formation and would result in substantially less CO formation. Again, a similar TON value (45 vs 42 TON at 72 h) and a similar reaction curve profile are observed with and without Hg^0 present. While this experiment does not confirm a molecular-active catalyst, the data is consistent with the molecular species.

Finally, dynamic light scattering (DLS) studies were done on the PCO_2RRs after 72 h of irradiation. Only two of the lowest TON value catalysts ($\mathbf{4}^{Cl}$ and $\mathbf{1}^{OH}\mathbf{1}^{BF4}$) show a moderate DLS signal between 2 nm and 800 nm sizes (Figure 5). A small signal is observed near 1 nm for $\mathbf{1}^{NTf2}$ and $\mathbf{1}^{OH}\mathbf{1}^{BF4}$ as well, although we note this is near the detection limit of the instrument, and assuming a spherical nanoparticle would only correspond to approximately 8 Au atoms if the entire particle was Au atoms face-centered-cubic-packed with a unit cell volume of 0.0679 nm^3.[64] Notably, the Au atom count of a particle would likely be smaller than this since DLS actually measures the hydrodynamic radius.[64] Combined, these three tests for heterogeneity suggest the catalysts may be functioning as molecular systems since the highest performing catalysts do not show evidence of forming heterogeneous species across three common heterogeneity tests. Lastly, the rate of catalysis was found to increase as the concentration of the $\mathbf{2}^{Cl}$ decreased (Figure 6). A TOF of up to 28.2 h^{-1} was reached at 0.1 μM of

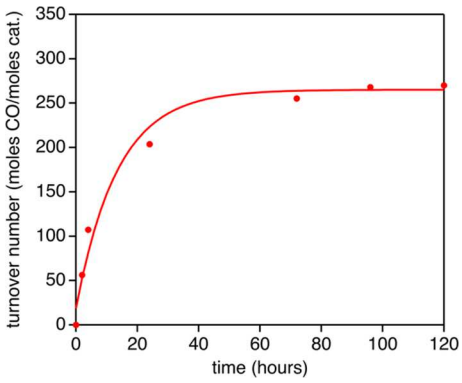

Figure 6. TON of CO versus time plot of complex $\mathbf{2}^{Cl}$ at 0.1 μM concentration.

$\mathbf{2}^{Cl}$ with a TON of 270 obtained at this concentration. The increase in TOF suggests that the rate of catalysis is limited by the amount of reductant [$Ir(ppy)_3^-$] in solution and that the catalysis being observed is homogeneous since a lower concentration would be expected to form nanoparticles more slowly than a higher concentration.

CONCLUSIONS

Eleven gold complexes bearing *N*-heterocyclic carbene ligands were tested for CO_2 reduction reactivity in a photosensitized system. The complexes were selected with an array of wingtip groups on the carbene ligand and with variations in labile ligands on the gold atoms. In general, the complexes were found to be durable in the photocatalytic CO_2 reduction reaction with catalysis continuing in many cases for ∼50 h with CO generation as the only product at >1 TON. The Au complexes with chloride atoms as the labile ligand were found to undergo rapid catalysis without an induction period, which indicates the chloride atom is rapidly dissociated upon reduction of the complex to give an active catalyst species. More tightly bound ligands such as phenyl and carbazole groups were slow to access the active catalyst without the use of acid additives. Additionally, the most active complex in the photocatalytic CO_2 reduction reaction was analyzed via the Maitlis test, the Hg^0 test, and DLS, which showed no evidence of heterogeneous behavior. The tunability of these catalysts with respect to TOFs and TON numbers via ligand substitutions is attractive toward future studies. Future efforts will focus on increasing the rate of photocatalysis while retaining the high durability.

EXPERIMENTAL SECTION

General Information. MeCN was freshly distilled over CaH_2 and kept under N_2 before use. DMF was distilled by vacuum distillation with heating to not more than 100 °C with no drying agent present. The presence of drying agents (CaH_2 or 4 Å MS) accelerates decomposition. DMF was distilled in 500 mL portions with the first 100 mL and the last 100 mL being discarded. The remaining 300 mL was kept under N_2 in a freezer and was not used for a period of more than 2 weeks before being discarded. $Ir(ppy)_3$ was purchased from Strem and used as received. Complexes $\mathbf{1}^{Cl}$,[47] $\mathbf{2}^{Cl}$,[47] $\mathbf{3}^{Cl}$,[48] $\mathbf{4}^{Cl}$,[47] $\mathbf{5}^{Cl}$,[47] $\mathbf{1}^{NTf2}$,[49] $\mathbf{1}^{OH}$,[49,50] $\mathbf{1}^{OH}\mathbf{1}^{BF4}$,[51] $\mathbf{1}^{Cz}$,[52] and $\mathbf{4}^{Ph}$[53] used herein were all prepared according to previously reported methods. BIH was

https://doi.org/10.1021/acs.inorgchem.2c03487
Inorg. Chem. 2022, 61, 18802−18809

prepared as previously described and recrystallized from hot EtOH/H_2O (2:1) prior to use.[43] TEA was freshly distilled over CaH_2 and kept under N_2 prior to use. Celite was obtained from Celite Corp. (545, not acid-washed) and used as received.

Activation with $AgBF_4$. The literature procedure was generally followed with some modifications as listed below.[55] $AgBF_4$ (1.25 equiv.) was added to a stirred solution of [Au(NHC)Cl] (1.0 equiv.) in dichloromethane (~0.03 M). The reaction mixture was stirred, avoiding the presence of light, at room temperature for 5 min and then filtered over Celite. The solvent was evaporated by passing N_2 over the solution, and the complex was then used directly in catalysis experiments.

Activation with HBF_4*Et_2O. The literature procedure was generally followed with some modifications as listed below.[53,56] HBF_4*Et_2O (1.1 equiv.) was added to a MeCN (~0.03 M) solution of $\mathbf{1}^{Cz}$ or $\mathbf{4}^{Ph}$ (1.0 equiv.), and the solution was stirred for 5 min at room temperature. The solvent was then removed under vacuum, diethyl ether was added, and the solution was filtered. The solid obtained was washed with Et_2O and dried. The above procedure was followed for $\mathbf{1}^{OH}$ except that the complex was first dissolved in toluene (0.09 M in catalyst), then acid was added, then MeCN (0.14 M in catalyst) was added, and the solution was stirred for 2 h. Pentane was added to precipitate $\mathbf{1}^{MeCN BF4}$. The liquid was removed by cannula and $\mathbf{1}^{MeCN BF4}$ was then dried under N_2.

PCO_2RR Setup. Photocatalytic experiments were performed in a 17 mL Pyrex culture tube (no. 99447, threaded GPI 15-415, 16 × 150 mm) with a stir bar by adding BIH (0.005 g, 0.02 mmol, 1×10^{-2} M), MeCN (6 mL), $Ir(ppy)_3$ (0.2 mL of a 1×10^{-3} M MeCN stock solution in a MeCN solution; final reaction concentration after degassing: 1×10^{-4} M), and catalyst (0.2 mL of a 1×10^{-5} M MeCN stock solution; final reaction concentration after degassing: 1×10^{-6} M). Each tube was sealed with a Teflon-coated rubber septum inside an open top screw cap with the parafilm sealed around the cap-to-tube joint. A white rubber septum (14/20 septum inverted) was placed over the cap, and the rubber septum was parafilm sealed to the Pyrex tube (see Figure S9). The mixture was then bubbled vigorously with CO_2 until the solution volume reached 1.9 mL (typically 15 min) and then 0.1 mL of N_2 degassed distilled triethylamine was injected into the mixture. A neutral white LED (Thorlabs, MNWHL4, color temperature: 4900 K) mounted with a collimation adaptor (Thorlabs, SM2F32-A, lens: Thorlabs, ACL50832U-A, with an antireflective coating over the range of 350−700 nm) was used as the light source for the photocatalytic experiments. The photocatalytic reaction vessel was set at a distance to adjust the power equal to 1 sun intensity across the white light emission range (380−750 nm), which was determined by using a power meter (Coherent PowerMax PM10 detector with a FieldMate 1098297 instrument). The sun intensity across the 380−750 nm range was calibrated using cut-off and cut-on filters with an AAA rated solar simulator with a reading of 180 mW on the power meter equaling 63.6 mW/cm^2 when accounting for the detector area.

PCO_2RR Product Detection. Product analysis via gas chromatography (GC) was done after 1, 2, 4, 24, 48, and 72 h of photolyzing the reaction. Then, headspace analysis was conducted with a VICI gas-tight syringe with a stopcock and a custom Agilent 7890B GC instrument equipped with an Agilent Porapak Q 6ft, 1/8 in. O.D. column, a methanizer, an FID detector, and a TCD detector. The amount of CO and CH_4 formed was quantified by using the FID detector signal, while H_2 was quantified using the TCD detector signal. All GC response calibrations were done using standards purchased from BuyCalGas.com. GC samples were prepared by taking headspace samples (300 μL) using a VICI gas-tight syringe, compressing the sealed sample to 250 μL, then submerging the tip of the sealed gas tight syringe in diethyl ether, opening and closing the valve to adjust the pressure in the syringe to atmospheric pressure, and injecting the sample into the GC instrument (see Figure S10 for a representative GC trace). Formate analysis was conducted as previously described by ^{1}H NMR spectroscopy (see Figure S11 for a representative formate analysis ^{1}H NMR trace).[40] Formate analysis was only performed at the end of the photocatalytic reaction as it requires significant reaction volume. No formate or methane was observed in these experiments. Only trace H_2 was observed, equaling less than 1 TON. All data points were collected in at least duplicate via two separate reactions. Data points agreed within a maximum of ±10% with a typical agreement of < ±5% being observed. Control experiments were conducted. Removal of the Au catalyst, CO_2, or BIH led to no CO formation. Removal of $Ir(ppy)_3$ led to small amounts (~1 TON as the highest observed) of CO formation after prolong irradiation with no appreciable CO forming in the first 24 h (Figure S12).

Heterogeneity Test Procedures. *Maitlis Test.*[61,62] A PCO_2RR reaction was setup as described above with GC monitoring. After 4 h, with GC evidence of typical reaction behavior indicating the presence of the active catalyst, the reaction was transferred via a cannula through a rubber septum (white rubber, 14/20 size) onto an in-line filter with a bed of Celite (~50 mL) resting on a fine frit with a filter paper on top of the Celite to reduce disruption of the Celite bed. The in-line filter with Celite and filter paper in place was previously thoroughly flame-dried under vacuum and then kept under N_2 for the duration of the experiment. The in-line filter was connected to an N_2-filled, flame-dried, two-neck flask with vacuum applied. Celite was rinsed with dry, distilled MeCN (5 mL). The reaction solution was then transferred via a cannula to the Pyrex reaction tube and degassed with CO_2 until the solution reached a volume of 2 mL. The solution was then photolyzed and monitored as described above. Notably, the concentration of triethylamine was likely diminished to some extent during the degassing phase, given the odor of the vapors coming off the exit needle.

Hg^0 Test.[62] A PCO_2RR reaction was done as described above with GC monitoring. After 4 h, with GC evidence of typical reaction behavior indicating the presence of the active catalyst, Hg^0 (0.5 mL) was injected into the reaction vessel via a syringe. The solution was then photolyzed and monitored as described above.

DLS Analysis. DLS analysis was conducted with a Malvern Instruments device (model: ZEN3600, serial no: MAL 1037566) by collecting a sample (2 mL) after the reaction had been photolyzed for 72 h. The sample was analyzed from 1 to 800 nm in a semimicrodisposable cuvettes (dimensions: 12.5 × 12.5 × 45 mm).

■ ASSOCIATED CONTENT

Supporting Information

The Supporting Information is available free of charge at https://pubs.acs.org/doi/10.1021/acs.inorgchem.2c03487.

Evaluation of different reaction solvents, TOF analysis, example reaction setup, example product analysis data, and control experiments (PDF)

■ AUTHOR INFORMATION

Corresponding Authors

Steven P. Nolan − *Department of Chemistry and Centre for Sustainable Chemistry, Ghent University, Ghent 9000, Belgium;* orcid.org/0000-0001-9024-2035; Email: steven.nolan@ugent.be

Jared H. Delcamp − *Department of Chemistry and Biochemistry, University of Mississippi, University Park 38677 Mississippi, United States;* orcid.org/0000-0001-5313-4078; Email: delcamp@olemiss.edu

Authors

Dinesh Nugegoda − *Department of Chemistry and Biochemistry, University of Mississippi, University Park 38677 Mississippi, United States;* orcid.org/0000-0002-5456-8940

Nikolaos V. Tzouras − *Department of Chemistry and Centre for Sustainable Chemistry, Ghent University, Ghent 9000, Belgium*

Complete contact information is available at:
https://pubs.acs.org/10.1021/acs.inorgchem.2c03487

Notes

The authors declare no competing financial interest.

■ ACKNOWLEDGMENTS

D.N. and J.H.D. thank the National Science Foundation (NSF award 2102511) for funding this research. Preliminary data were collected under the NSF award 1800281. For the work performed in Ghent, we gratefully acknowledge VLAIO (SBO project CO2PERATE); the Special Research Fund (BOF) of Ghent University is also acknowledged for the Doctoral Scholarship (01D14919) to N.V.T. and starting and project grants to S.P.N. The Research Foundation—Flanders (FWO) is also gratefully acknowledged for a Fundamental Research PhD fellowship to N.V.T. (11I6921N). Umicore AG is thankfully acknowledged for the generous gift of materials.

■ REFERENCES

(1) Kojima, T. Photocatalytic Carbon Dioxide Reduction Using Nickel Complexes as Catalysts. *ChemPhotoChem* **2021**, *5*, 512−520.
(2) Kumaravel, V.; Bartlett, J.; Pillai, S. C. Photoelectrochemical Conversion of Carbon Dioxide (CO_2) into Fuels and Value-Added Products. *ACS Energy Lett.* **2020**, *5*, 486−519.
(3) Zhang, B.; Sun, L. Artificial Photosynthesis: Opportunities and Challenges of Molecular Catalysts. *Chem. Soc. Rev.* **2019**, *48*, 2216−2264.
(4) Dalle, K. E.; Warnan, J.; Leung, J. J.; Reuillard, B.; Karmel, I. S.; Reisner, E. Electro- and Solar-Driven Fuel Synthesis with First Row Transition Metal Complexes. *Chem. Rev.* **2019**, *119*, 2752−2875.
(5) Kuramochi, Y.; Ishitani, O.; Ishida, H. Reaction Mechanisms of Catalytic Photochemical CO_2 Reduction Using Re(I) and Ru(II) Complexes. *Coord. Chem. Rev.* **2018**, *373*, 333−356.
(6) White, J. L.; Baruch, M. F.; Pander, J. E., III; Hu, Y.; Fortmeyer, I. C.; Park, J. E.; Zhang, T.; Liao, K.; Gu, J.; Yan, Y.; Shaw, T. W.; Abelev, E.; Bocarsly, A. B. Light-Driven Heterogeneous Reduction of Carbon Dioxide: Photocatalysts and Photoelectrodes. *Chem. Rev.* **2015**, *115*, 12888−12935.
(7) Artero, V.; Fontecave, M. Solar Fuels Generation and Molecular Systems: Is It Homogeneous or Heterogeneous Catalysis? *Chem. Soc. Rev.* **2013**, *42*, 2338−2356.
(8) Hammer, N. I.; Sutton, S.; Delcamp, J. H.; Graham, J. D. Photocatalytic Water Splitting and Carbon Dioxide Reduction. In *Handbook of Climate Change Mitigation and Adaptation*; Chen, W. Y., Suzuki, T., Lackner, M., Eds.; Springer, 2017.
(9) Morris, A. J.; Meyer, G. J.; Fujita, E. Molecular Approaches to the Photocatalytic Reduction of Carbon Dioxide for Solar Fuels. *Acc. Chem. Res.* **2009**, *42*, 1983−1994.
(10) Sahara, G.; Ishitani, O. Efficient Photocatalysts for CO_2 Reduction. *Inorg. Chem.* **2015**, *54*, 5096−5104.
(11) Li, Z.; Brouwer, C.; He, C. Gold-Catalyzed Organic Transformations. *Chem. Rev.* **2008**, *108*, 3239−3265.
(12) de Frémont, P.; Marion, N.; Nolan, S. P. Cationic NHC−Gold(I) Complexes: Synthesis, Isolation, and Catalytic Activity. *J. Organomet. Chem.* **2009**, *694*, 551−560.
(13) Gaillard, S.; Cazin, C. S. J.; Nolan, S. P. N-Heterocyclic Carbene Gold(I) and Copper(I) Complexes in C−H Bond Activation. *Acc. Chem. Res.* **2012**, *45*, 778−787.
(14) A C A Bayrakdar, T. A. C. A.; Scattolin, T.; Ma, X.; Nolan, S. P. Dinuclear Gold(I) Complexes: From Bonding to Applications. *Chem. Soc. Rev.* **2020**, *49*, 7044−7100.
(15) Chintawar, C. C.; Yadav, A. K.; Kumar, A.; Sancheti, S. P.; Patil, N. T. Divergent Gold Catalysis: Unlocking Molecular Diversity through Catalyst Control. *Chem. Rev.* **2021**, *121*, 8478−8558.
(16) Ciriminna, R.; Falletta, E.; Della Pina, C.; Teles, J. H.; Pagliaro, M. Industrial Applications of Gold Catalysis. *Angew. Chem., Int. Ed.* **2016**, *55*, 14210−14217.
(17) Collado, A.; Nelson, D. J.; Nolan, S. P. Optimizing Catalyst and Reaction Conditions in Gold(I) Catalysis-Ligand Development. *Chem. Rev.* **2021**, *121*, 8559−8612.
(18) Gorin, D. J.; Toste, F. D. Relativistic Effects in Homogeneous Gold Catalysis. *Nature* **2007**, *446*, 395−403.
(19) Hashmi, A. S. The Catalysis Gold Rush: New Claims. *Angew. Chem., Int. Ed.* **2005**, *44*, 6990−6993.
(20) Hashmi, A. S. K. Gold-Catalyzed Organic Reactions. *Chem. Rev.* **2007**, *107*, 3180−3211.
(21) Hendrich, C. M.; Sekine, K.; Koshikawa, T.; Tanaka, K.; Hashmi, A. S. K. Homogeneous and Heterogeneous Gold Catalysis for Materials Science. *Chem. Rev.* **2021**, *121*, 9113−9163.
(22) Joost, M.; Amgoune, A.; Bourissou, D. Reactivity of Gold Complexes Towards Elementary Organometallic Reactions. *Angew. Chem., Int. Ed.* **2015**, *54*, 15022−15045.
(23) Lu, Z.; Li, T.; Mudshinge, S. R.; Xu, B.; Hammond, G. B. Optimization of Catalysts and Conditions in Gold(I) Catalysis-Counterion and Additive Effects. *Chem. Rev.* **2021**, *121*, 8452−8477.
(24) Marion, N.; Nolan, S. P. N-Heterocyclic Carbenes in Gold Catalysis. *Chem. Soc. Rev.* **2008**, *37*, 1776−1782.
(25) Nijamudheen, A.; Datta, A. Gold-Catalyzed Cross-Coupling Reactions: An Overview of Design Strategies, Mechanistic Studies, and Applications. *Chem. Eur. J.* **2020**, *26*, 1442−1487.
(26) Nolan, S. P. The Development and Catalytic Uses of N-Heterocyclic Carbene Gold Complexes. *Acc. Chem. Res.* **2011**, *44*, 91−100.
(27) Praveen, C. Carbophilic Activation of π-Systems Via Gold Coordination: Towards Regioselective Access of Intermolecular Addition Products. *Coord. Chem. Rev.* **2019**, *392*, 1−34.
(28) Hopkinson, M. N.; Richter, C.; Schedler, M.; Glorius, F. An Overview of N-Heterocyclic Carbenes. *Nature* **2014**, *510*, 485−496.
(29) Davis, S.; Nugegoda, D.; Tropp, J.; Azoulay, J. D.; Delcamp, J. H. Molecular Au(I) Complexes in the Photosensitized Photocatalytic CO_2 Reduction Reaction. *MRS Commun.* **2020**, *10*, 252−258.
(30) Chen, Y.; Li, C. W.; Kanan, M. W. Aqueous CO_2 Reduction at Very Low Overpotential on Oxide-Derived Au Nanoparticles. *J. Am. Chem. Soc.* **2012**, *134*, 19969−19972.
(31) Kauffman, D. R.; Alfonso, D.; Matranga, C.; Qian, H.; Jin, R. Experimental and Computational Investigation of Au25 Clusters and CO_2: A Unique Interaction and Enhanced Electrocatalytic Activity. *J. Am. Chem. Soc.* **2012**, *134*, 10237−10243.
(32) Sun, K.; Cheng, T.; Wu, L.; Hu, Y.; Zhou, J.; Maclennan, A.; Jiang, Z.; Gao, Y.; Goddard, W. A., 3rd; Wang, Z. Ultrahigh Mass Activity for Carbon Dioxide Reduction Enabled by Gold-Iron Core-Shell Nanoparticles. *J. Am. Chem. Soc.* **2017**, *139*, 15608−15611.
(33) Zhu, W.; Michalsky, R.; Metin, O.; Lv, H.; Guo, S.; Wright, C. J.; Sun, X.; Peterson, A. A.; Sun, S. Monodisperse Au Nanoparticles for Selective Electrocatalytic Reduction of CO_2 to CO. *J. Am. Chem. Soc.* **2013**, *135*, 16833−16836.
(34) Kim, H.; Park, H. S.; Hwang, Y. J.; Min, B. K. Surface-Morphology-Dependent Electrolyte Effects on Gold-Catalyzed Electrochemical CO_2 Reduction. *J. Phys. Chem. C* **2017**, *121*, 22637−22643.
(35) Cao, Z.; Kim, D.; Hong, D.; Yu, Y.; Xu, J.; Lin, S.; Wen, X.; Nichols, E. M.; Jeong, K.; Reimer, J. A.; Yang, P.; Chang, C. J. A Molecular Surface Functionalization Approach to Tuning Nanoparticle Electrocatalysts for Carbon Dioxide Reduction. *J. Am. Chem. Soc.* **2016**, *138*, 8120−8125.
(36) Jupally, V. R.; Dharmaratne, A. C.; Crasto, D.; Huckaba, A. J.; Kumara, C.; Nimmala, P. R.; Kothalawala, N.; Delcamp, J. H.; Dass, A. $Au_{137}(SR)_{56}$ Nanomolecules: Composition, Optical Spectroscopy, Electrochemistry and Electrocatalytic Reduction of CO_2. *Chem. Commun.* **2014**, *50*, 9895−9898.
(37) Qiao, J.; Liu, Y.; Hong, F.; Zhang, J. A Review of Catalysts for the Electroreduction of Carbon Dioxide to Produce Low-Carbon Fuels. *Chem. Soc. Rev.* **2014**, *43*, 631−675.

(38) Collado, A.; Gómez-Suárez, A.; Webb, P. B.; Kruger, H.; Bühl, M.; Cordes, D. B.; Slawin, A. M.; Nolan, S. P. Trapping Atmospheric CO_2 with Gold. *Chem. Commun.* **2014**, *50*, 11321−11324.
(39) Kelly, R. A., III; Clavier, H.; Giudice, S.; Scott, N. M.; Stevens, E. D.; Bordner, J.; Samardjiev, I.; Hoff, C. D.; Cavallo, L.; Nolan, S. P. Determination of N-Heterocyclic Carbene (NHC) Steric and Electronic Parameters Using the [(NHC)Ir(CO)$_2$Cl] System. *Organometallics* **2008**, *27*, 202−210.
(40) Rodrigues, R. R.; Boudreaux, C. M.; Papish, E. T.; Delcamp, J. H. Photocatalytic Reduction of CO_2 to CO and Formate: Do Reaction Conditions or Ruthenium Catalysts Control Product Selectivity? *ACS Appl. Energy Mater.* **2019**, *2*, 37−46.
(41) Tamaki, Y.; Koike, K.; Morimoto, T.; Ishitani, O. Substantial Improvement in the Efficiency and Durability of a Photocatalyst for Carbon Dioxide Reduction Using a Benzoimidazole Derivative as an Electron Donor. *J. Catal.* **2013**, *304*, 22−28.
(42) Shirley, H.; Figgins, M. T.; Boudreaux, C. M.; Liyanage, N. P.; Lamb, R. W.; Webster, C. E.; Papish, E. T.; Delcamp, J. H. Impact of the Dissolved Anion on the Electrocatalytic Reduction of CO_2 to CO with Ruthenium CNC Pincer Complexes. *ChemCatChem* **2020**, *12*, 4879−4885.
(43) Huckaba, A. J.; Sharpe, E. A.; Delcamp, J. H. Photocatalytic Reduction of CO_2 with Re-Pyridyl-NHCs. *Inorg. Chem.* **2016**, *55*, 682−690.
(44) Agarwal, J.; Shaw, T. W.; Stanton, C. J., 3rd; Majetich, G. F.; Bocarsly, A. B.; Schaefer, H. F., 3rd NHC-Containing Manganese(I) Electrocatalysts for the Two-Electron Reduction of CO_2. *Angew. Chem., Int. Ed.* **2014**, *53*, 5152−5155.
(45) Jin, T.; He, D.; Li, W.; Stanton, C. J.; Pantovich, S. A.; Majetich, G. F.; Schaefer, H. F.; Agarwal, J.; Wang, D.; Li, G. CO_2 Reduction with Re(I)-NHC Compounds: Driving Selective Catalysis with a Silicon Nanowire Photoelectrode. *Chem. Commun.* **2016**, *52*, 14258−14261.
(46) Agarwal, J.; Shaw, T. W.; Schaefer, H. F., III; Bocarsly, A. B. Design of a Catalytic Active Site for Electrochemical CO_2 Reduction with Mn(I)-Tricarbonyl Species. *Inorg. Chem.* **2015**, *54*, 5285−5294.
(47) Fremont, P. D.; Scott, N. M.; Stevens, E. D.; Nolan, S. P. Synthesis and Structural Characterization of N-Heterocyclic Carbene Gold(I) Complexes. *Organometallics* **2005**, *24*, 2411−2418.
(48) Collado, A.; Gómez-Suárez, A.; Martin, A. R.; Slawin, A. M.; Nolan, S. P. Straightforward Synthesis of [Au(NHC)X] (NHC = N-Heterocyclic Carbene, X = Cl, Br, I) Complexes. *Chem. Commun.* **2013**, *49*, 5541−5543.
(49) Gaillard, S.; Slawin, A. M.; Nolan, S. P. A N-Heterocyclic Carbene Gold Hydroxide Complex: A Golden Synthon. *Chem. Commun.* **2010**, *46*, 2742−2744.
(50) Nahra, F.; Patrick, S. R.; Collado, A.; Nolan, S. P. A Novel Route for Large-Scale Synthesis of [Au(NHC)(OH)] Complexes. *Polyhedron* **2014**, *84*, 59−62.
(51) Nahra, F.; Tzouras, N. V.; Collado, A.; Nolan, S. P. Synthesis of N-Heterocyclic Carbene Gold(I) Complexes. *Nat. Protoc.* **2021**, *16*, 1476−1493.
(52) Tzouras, N. V.; Martynova, E. A.; Ma, X.; Scattolin, T.; Hupp, B.; Busen, H.; Saab, M.; Zhang, Z.; Falivene, L.; Pisanò, G.; Van Hecke, K. V.; Cavallo, L.; Cazin, C. S. J.; Steffen, A.; Nolan, S. P. Simple Synthetic Routes to Carbene-M-Amido (M=Cu, Ag, Au) Complexes for Luminescence and Photocatalysis Applications. *Chem.—Eur. J.* **2021**, *27*, 11904−11911.
(53) Tzouras, N. V.; Saab, M.; Janssens, W.; Cauwenbergh, T.; Van Hecke, K.; Nahra, F.; Nolan, S. P. Simple Synthetic Routes to N-Heterocyclic Carbene Gold(I)-Aryl Complexes: Expanded Scope and Reactivity. *Chem.—Eur. J.* **2020**, *26*, 5541−5551.
(54) Carpenter, C. A.; Brogdon, P.; McNamara, L. E.; Tschumper, G. S.; Hammer, N. I.; Delcamp, J. H. A Robust Pyridyl-NHC-Ligated Rhenium Photocatalyst for CO_2 Reduction in the Presence of Water and Oxygen. *Inorganics* **2018**, *6*, 22.
(55) Gómez-Suárez, A.; Ramón, R. S.; Slawin, A. M.; Nolan, S. P. Synthetic Routes to [Au(NHC)(OH)] (NHC = N-Heterocyclic Carbene) Complexes. *Dalton Trans.* **2012**, *41*, 5461−5463.
(56) Ramón, R. S.; Gaillard, S.; Poater, A.; Cavallo, L.; Slawin, A. M.; Nolan, S. P. [{Au(IPr)}2(Mμ-OH)]X Complexes: Synthetic, Structural and Catalytic Studies. *Chem.—Eur. J.* **2011**, *17*, 1238−1246.
(57) Shirley, H.; Su, X.; Sanjanwala, H.; Talukdar, K.; Jurss, J. W.; Delcamp, J. H. Durable Solar-Powered Systems with Ni-Catalysts for Conversion of CO_2 or CO to CH_4. *J. Am. Chem. Soc.* **2019**, *141*, 6617−6622.
(58) Bonin, J.; Robert, M.; Routier, M. Selective and Efficient Photocatalytic CO_2 Reduction to CO Using Visible Light and an Iron-Based Homogeneous Catalyst. *J. Am. Chem. Soc.* **2014**, *136*, 16768−16771.
(59) Guo, Z.; Yu, F.; Yang, Y.; Leung, C.-F.; Ng, S.-M.; Ko, C.-C.; Cometto, C.; Lau, T.-C.; Robert, M. Photocatalytic Conversion of CO_2 to CO by a Copper(II) Quaterpyridine Complex. *ChemSusChem* **2017**, *10*, 4009−4013.
(60) Thoi, V. S.; Kornienko, N.; Margarit, C. G.; Yang, P.; Chang, C. J. Visible-Light Photoredox Catalysis: Selective Reduction of Carbon Dioxide to Carbon Monoxide by a Nickel N-Heterocyclic Carbene-Isoquinoline Complex. *J. Am. Chem. Soc.* **2013**, *135*, 14413−14424.
(61) Hamlin, J. E.; Hirai, K.; Gibson, V. C.; Maitlis, P. M. Pentamethylcyclopentadienyl—Rhodium and —Iridium Complexes: Part 35. Hydrogenation Catalysts Based on $[(RhC_5Me_5)_2(OH)_3]^+$ and the Border between Homogeneous and Heterogeneous Systems. *J. Mol. Catal.* **1982**, *15*, 337−347.
(62) Widegren, J. A.; Finke, R. G. A Review of the Problem of Distinguishing True Homogeneous Catalysis from Soluble or Other Metal-Particle Heterogeneous Catalysis under Reducing Conditions. *J. Mol. Catal. Chem.* **2003**, *198*, 317−341.
(63) Britton, G. T.; McBain, J. W. Amalgams for Gold and Mercury. *J. Am. Chem. Soc.* **1926**, *48*, 593−598.
(64) Uddin, J.; Rahman, A.; Ghann, W.; Kang, H.; Rahman, A. K. Terahertz Multispectral Imaging for the Analysis of Gold Nanoparticles' Size and the Number of Unit Cells in Comparison with Other Techniques. *Int. J. Biosen. Bioelectron.* **2018**, *4*, 159−164.

https://doi.org/10.1021/acs.inorgchem.2c03487
Inorg. Chem. 2022, 61, 18802−18809